Characterization of Light Transport in Scattering Media at Subdiffusion Length Scales with Low-Coherence Enhanced Backscattering

Vladimir Turzhitsky, Jeremy D. Rogers, Nikhil N. Mutyal, Hemant K. Roy, and Vadim Backman

(Invited Paper)

***Abstract*—Low-coherence enhanced backscattering (LEBS) is a technique that has recently shown promise for tissue characterization and the detection of early precancer. Although several Monte Carlo models of LEBS have been described, these models have not been accurate enough to predict all of the experimentally observed LEBS features. We present an appropriate Monte Carlo model to simulate LEBS peak properties from polystyrene microsphere suspensions in water. Results show that the choice of the phase function greatly impacts the accuracy of the simulation when the transport mean free path (ls^*) is much greater than the spatial coherence length (L_{SC}). When $ls^* < L_{SC}$, a diffusion-approximation-based model of LEBS is sufficiently accurate. We also use the Monte Carlo model to validate that LEBS can be used to measure the radial scattering probability distribution (radial point spread function), $p(r)$, at small length scales and demonstrate LEBS measurements of $p(r)$ from biological tissue. In particular, we show that precancerous and benign mucosal tissues have different small length scale light transport properties.**

***Index Terms*—Enhanced backscattering, cancer detection, light Monte Carlo, spatial coherence, tissue characterization.**

I. Introduction

ENHANCED backscattering (EBS) is one of the two self-interference phenomena observed when a sample is illuminated with a coherent light source. The enhanced backscattering effect, also known as coherent backscattering, manifests as an enhancement of intensity in the backward direction of the incident light. This effect was initially tied with weak localization of electrons, and later extended to optical waves [1]. Further theoretical and experimental work uncovered that EBS can be used to measure the optical properties of diffusely scattering media [2], [3]. The width of the coherent backscattering peak was found to be proportional to λ/ls^*, where λ is the wavelength and ls^* is the transport mean free path. However, due to the inherent challenges in this method, the utilization of this phenomenon for characterizing biological tissue has been hampered until recent years.

The second self-interference phenomenon, known as speckle, is one of the primary impediments to measuring enhanced backscattering from tissue. The large amplitude and ubiquity of the speckle pattern overwhelms the coherent backscattering signal in solid samples. This is why early studies primarily utilized liquid suspensions of particles such that the Brownian motion inside the sample provides a large number of ensembles, all of which are averaged within a single acquisition of the detector. The lack of Brownian motion in biological tissue requires the averaging of many ensembles by moving the entire sample. Furthermore, the narrow line shape of the coherent backscattering peak from tissue requires high angular resolution detection capable of resolving signals on the order of 0.001°.

The extension of enhanced backscattering into the partial spatial coherence regime was first explored by Kim *et al.* [4] and provides several advantages that make the technique amenable for tissue characterization. The technique overcomes the difficulties of measuring enhanced backscattering from tissue by broadening the coherent backscattering peak by several orders of magnitude and virtually eliminating the speckle noise.

The new method also offers further advantages that are essential for the biomedical application of enhanced backscattering. The reduced spatial coherence results in a depth selective signal by removing the contribution of light at longer scattered radii [5], [6]. The addition of spectrally resolved detection allows for obtaining the interference phenomenon from a range of wavelengths, adding an extra dimension for more complete characterization of tissue properties [7]. Thus far, low-coherence enhanced backscattering (LEBS) has shown promise for the early detection of colorectal cancer [8] and pancreatic cancer [9], [10] by the quantification of superficial tissue layer changes that are unapparent from conventional histology.

Earlier work in characterizing LEBS has revealed that the dependencies of the peak width and enhancement factor on sample properties are more complicated than those of EBS [4]. For example, the LEBS peak width was found to have three ls^* dependent regimes with distinctly different behaviors for varying

Manuscript received July 19, 2009; revised August 28, 2009; accepted September 2, 2009. Date of publication October 30, 2009; date of current version June 4, 2010. This work was supported in part by R01 EB003682, in part by R01 CA112315, and in part by R01 CA128641.

V. Turzhitsky, J. D. Rogers, and N. N. Mutyal are with the Department of Biomedical Engineering, Northwestern University, Evanston, IL 60208 USA (e-mail: vt@u.northwestern.edu; jdrogers@northwestern.edu; nikhilmutyal2012@u.northwestern.edu).

H. K. Roy is with the Department of Internal Medicine, NorthShore University HealthSystems, Evanston, IL 60201 USA, and also with Pritzker School of Medicine, University of Chicago, Chicago, IL 60637 USA (e-mail: h-roy @northwestern.edu).

V. Backman is with the Department of Biomedical Engineering, Northwestern University, Evanston, IL 60208 USA, and also with Robert H. Lurie Comprehensive Cancer Institute, Chicago, IL 60611 USA. He is also with the Division of Gastroenterology, NorthShore University HealthSystems, Evanston, IL 60201 USA (e-mail: v-backman@northwestern.edu).

Color versions of one or more of the figures in this paper are available online at http://ieeexplore.ieee.org.

Digital Object Identifier 10.1109/JSTQE.2009.2032666

values of the anisotropy factor (g) [7], this being very different from the λ/ls* relationship seen in EBS. The enhancement factor, defined as the relative height of the peak, was also found to be dependent on the mean free path of the medium. On the other hand, the enhancement factor of EBS has no dependence on the mean free path of the sample.

These experimental findings combined with the demonstrated diagnostic potential of the LEBS measurement have motivated several groups to develop Monte Carlo [11], [12] and theoretical [6], [12] models for the simulation and understanding of LEBS. Although these Monte Carlo models have given insight into important properties such as the penetration depth of the LEBS signal [6], a good correspondence between the experimental peak properties, including peak width and enhancement factor, with a simulated result has not been demonstrated until now.

In the following sections, this paper will discuss the experimental and modeling methodologies required to obtain agreement between simulated and experimental peak properties. We will present experimental and Monte Carlo results that illustrate the dependence of the LEBS peak width and enhancement factor on optical properties and the spatial coherence length. We will then present a diffusion-based model for LEBS, which can be accurate in certain conditions. Finally, we will apply LEBS as a technique for measuring the scattering probability distribution, $p(r)$, at small length scales.

II. Materials and Methods

A. Theoretical Background

A random medium illuminated by a uniform plane wave will backscatter a fraction of the reflected power in the reverse direction of the incident beam. The principle of the reversibility of light paths states that there must also be an equivalent fraction of the incident beam that traverses an identical path in the opposite direction. The light from these time-reversed paths will have an identical phase and therefore constructively interfere at the exact backward direction when the angular distribution of backscattered light is observed. For angles away from the backward direction, the interference depends on the phase difference which intern depends on the backscattering angle and location at which the partial waves exit the medium.

The resulting peak can be described as a summation of interference patterns observed from a series of Young's double pinhole experiments, where the distances between the pinholes are the exit locations of all of the possible time-reversed path pairs. The shape of the enhanced backscattering peak in a nonabsorbent medium therefore depends on the point spread function of light at the tissue surface in the 0° backward direction (i.e., 180° with respect to the direction of the incident light), termed $p(r)$, with a 2-D Fourier transform relationship:

$$I(\theta) = \iint p(\vec{r}) \exp(ik\vec{r}\sin(\theta)) d^2 r \tag{1}$$

where θ is the angle between the incident wave vector and the backscattered wave vector and k is the wavenumber. The sinusoidal oscillations obtained in Young's double pinhole experiment can be obtained by substituting $p(r)$ with a pair of delta functions into (1). Thus, the width of the EBS cone is inversely related to the average backscattering exit radius of the beam. This average distance is proportional to ls*. When the diffusion approximation is used to model the shape of $p(r)$, the EBS peak shape is approximated by [2]

$$I_{\mathrm{EBS}}(\theta) \approx \frac{3}{8\pi} \left[\begin{array}{c} 1 + \dfrac{2z_0}{\mathrm{ls}^*} + \dfrac{1}{(1+k\theta \mathrm{ls}^*)^2} \\ \times \left(1 + \dfrac{1 - \exp(-2k\theta z_0)}{k\theta \mathrm{ls}^*} \right) \end{array} \right] \tag{2}$$

where z_0 is the location of the trapping plane.

The requirement in (1) and (2) is that all path pairs incident on the scattering medium are fully coherent. Under partial spatial coherence illumination, the interference depends on the separation distance of the path pairs and the degree of spatial coherence $c(r)$. In this case

$$I_{\mathrm{LEBS}}(\theta) = \iint p(\vec{r}) c(\vec{r}) \exp(ik\vec{r}\sin(\theta)) d^2 r. \tag{3}$$

When $p(r)$ is radially symmetric, the 2-D Fourier transform can be written as

$$I_{\mathrm{LEBS}}(\theta) = \int_0^\infty 2\pi r p(r) c(r) J_0(kr\sin(\theta)) dr \tag{4}$$

where J_0 is the zero-order Bessel function of the first kind. A symmetric $p(r)$ will result when the illumination has normal incidence on the sample and either unpolarized or circularly polarized illumination is used.

When the degree of spatial coherence extends much farther than ls*, the diffusion approximation that is conventionally used to model EBS can be extended to model the LEBS signal. This can be done by either substituting the diffusion approximation $p(r)$ into (3) or by applying the convolution theorem

$$I_{\mathrm{LEBS}}(\theta) = \mathrm{FT}[p(r) \cdot c(r)] = I_{\mathrm{EBS}}(\theta) * S(\theta) \tag{5}$$

where $S(\theta)$ is the Fourier transform of $c(r)$ and, equivalently, the angular profile of the source from the sample surface. By substituting (2) into (5), a diffusion approximation for the LEBS signal is obtained.

The properties of $p(r)$ uniquely characterize the scattering media and determine the shape of the peak. The shape of $p(r)$ at $r < \mathrm{ls}^*$ has not been investigated in tissue due to the lack of an effective technique to measure this signal, despite the fact that scattering properties in this region can be sensitive to characteristics of the phase function. From (3) and (5), $p(r)$ can be found from the inverse Fourier transform of the angular profile of an LEBS peak

$$p(r) = \frac{\mathrm{FT}^{-1}[I_{\mathrm{LEBS}}(\theta)]}{c(r)}. \tag{6}$$

As $c(r)$ approaches 0, the measurement becomes dominated by noise and is no longer accurate. The use of LEBS allows the weight of the collected signal to be concentrated at small values of r, yielding a more accurate measurement of $p(r)$ for small r (i.e., $r < \mathrm{ls}^*$) than what is possible with any other available method.

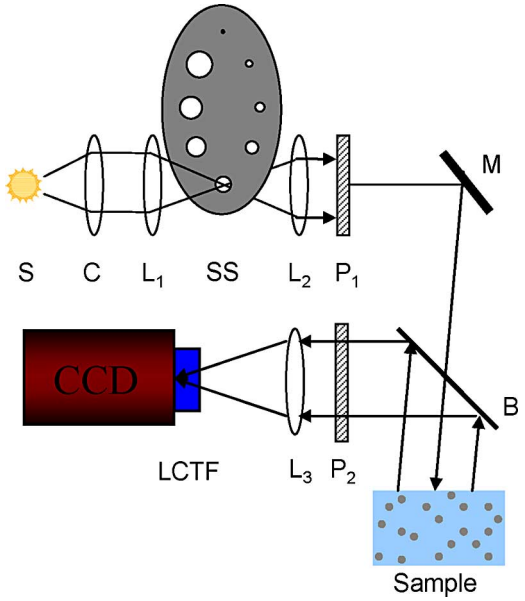

Fig. 1. Schematic of LEBS experimental instrument. A broadband 450-W Xenon source (S) is imaged onto an aperture of variable size that serves as a secondary source (SS). The size of the aperture is selected by appropriately positioning the aperture wheel. The beam is collimated with lens L_2 and passed through polarizer P_1. A beam splitter (B) allows collection of backscattered light from the sample. The copolarized light is selected with polarized P_2. Lens L_3 then maps the angular distribution of the backscattered light onto the CCD camera detection chip. An LCTF attached to the camera is used to select the wavelength of collection.

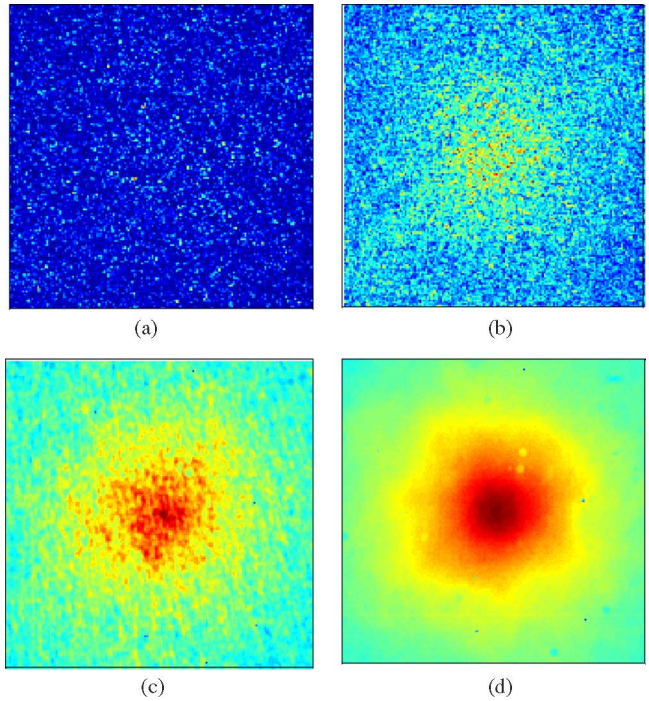

Fig. 2. Demonstration of speckle reduction in LEBS from a dried paint sample ($ls^* \sim 4\ \mu$m). (a) EBS measurement obtained with helium–neon (HeNe) laser. (b) Average of 30 ensembles of EBS measurements collected with HeNe laser. The EBS signal begins to be visible over the speckle noise. (c) Single measurement with partial coherence illumination ($L_{SC} = 160\ \mu$m). (d) Single measurement with partial coherence measurement ($L_{SC} = 20\ \mu$m).

B. Experiment

A schematic of the experimental setup used in earlier LEBS studies has been described in previous literature [4], [5], [7]. A modified experimental setup that simplifies alignment and improves sampling was implemented in the experimental studies discussed in this paper. A schematic of the setup is shown in Fig. 1. A broadband 450 W Xe Oriel light source (Newport Corporation, Stratford, CT) relayed with a series of lenses onto a high-power tungsten aperture that is positioned within an aperture wheel. The aperture acts as a secondary source of variable size that is then collimated by a lens ($f = 200$ mm). The degree of spatial coherence and the spatial coherence length (L_{SC}) is determined according to the Van Cittert–Zernike theorem as [13]

$$c(r) = \frac{2J_1(r/L_{SC})}{r/L_{SC}}$$

$$L_{SC} = \frac{\lambda}{\pi\alpha} \tag{7}$$

where J_1 is the first-order Bessel function of the first kind, λ is the wavelength, and α is the angular extent of the source. In the described setup, α is determined from the ratio of the diameter of the secondary source to the focal length of the collimating lens L_2 (see Fig. 1). The assumption made for this calculation is that the secondary source is completely incoherent and has a uniform circular intensity profile. The contribution of the phase term in the coherence function can be neglected because the phase difference between points within the illumination area is small due the use of a collimating lens [13]. The collimated beam is passed through a beam splitter onto the sample and a Fourier lens ($f = 100$ mm) is positioned at a reflecting face of the beam splitter. The wavelength of backscattered light is selected with a Liquid crystal tunable filter (Varispec, CRi, Inc., Woburn, MA). The angular distribution is mapped onto the CCD camera chip (PIXIS 400B, Princeton Instruments).

The setup in Fig. 1 has two advantages over the earlier LEBS systems: 1) the alignment is not disrupted when the spatial coherence is changed by rotating the aperture wheel to a different position, and 2) the LEBS peak is not sampled with a spectrometer slit, allowing for higher resolution imaging of the entire backscattered cone. As an example of one of the advantages of enhanced backscattering measurement with partially coherent light, Fig. 2 illustrates the speckle reduction capability of LEBS with backscattering measurement obtained from dried paint. In Fig. 2(a), a coherent backscattering measurement from the solid sample is shown to be completely submerged in speckle. An EBS peak begins to be visible in Fig. 2(b), where 30 measurements at various positions in the sample are averaged. For comparison, only a single measurement is required to see the LEBS peak under partial coherence illumination, as shown in Fig. 2(c) and (d) for $L_{SC} = 160\ \mu$m and $L_{SC} = 20\ \mu$m, respectively.

The LEBS peak was characterized for a variety of illumination conditions from measurements on polystyrene microsphere suspensions in water. Microspheres of sizes ranging from 0.36 to 0.65 μm (Duke scientific) were used to obtain a range of g values between 0.71 and 0.86. The samples were made to approximate a semiinfinite media by maintaining the thickness and the

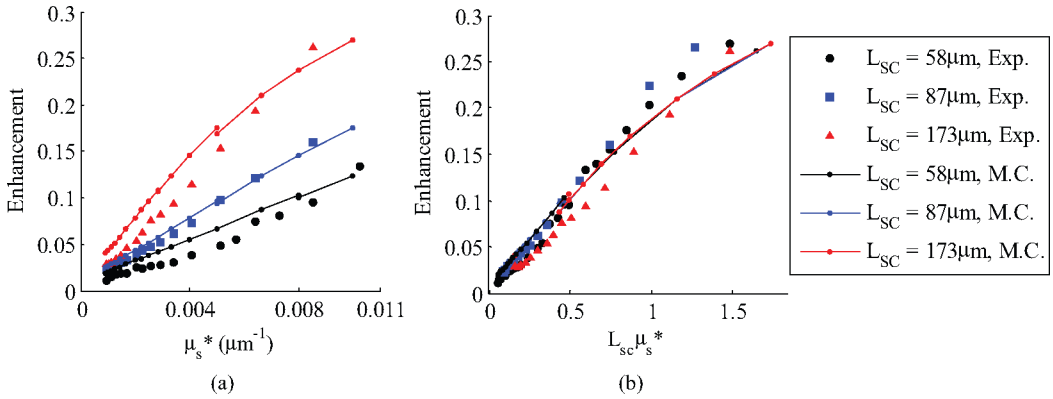

Fig. 3. Enhancement factor as a function of μ_s^* for varying L_{SC} ($g = 0.86$). (a) Enhancement factor is shown to have three distinct dependencies on μ_s^* for three values of L_{SC}. (b) Three dependencies coincide when enhancement factor is plotted against $L_{SC}\mu_s^*$. The Monte Carlo results (lines) show the same dependencies as the experimental results (symbols).

diameter of the sample more than 50·ls*. These suspensions were diluted to varying concentrations in order to achieve values of ls* in the range of 20–1100 μm. Measurements were obtained at $\lambda = 680$ nm and all optical properties were calculated with Mie theory. The image obtained with the CCD camera was background subtracted and normalized by an intensity measurement collected from a spectralon white reflectance standard (Ocean Optics, Dunedin, FL). The incoherent baseline was subtracted by fitting a plane to the signal at the periphery of the peak. The enhancement factor of the LEBS peak was therefore bounded between 0 and 1. The LEBS peak width was measured as the full-width at half maximum of the signal after averaging over the azimuth angle.

In order to illustrate the potential of $p(r)$ measurements from tissue with LEBS, an animal study utilizing eight rats was performed. Four of these rats were treated with azoxymethane (AOM), a carcinogen that induces cancerous changes typically around 20–40 weeks after treatment. The remaining four rats were injected with saline and served as controls. The rats were sacrificed 10 weeks after the injection and LEBS measurements were obtained for $L_{SC} = 87$ μm from four to five sites per rat. The LEBS peaks in each group were averaged and the inverse Fourier transform relationship [(6) was used to calculate $p(r)$ for values of r up to the point were the degree of spatial coherence dropped below the half maximum ($\sim 2.2 \cdot L_{SC}$)].

C. Polarized Light Monte Carlo Simulation of LEBS

The LEBS phenomenon was modeled with polarized light Monte Carlo simulations. A publicly available Monte Carlo code [14], [15] was used to simulate the scattering properties of polystyrene microsphere suspensions in water. The code was modified to store small-angle backscattered rays from 0° to 2° following previously reported methodology [11]. A finite range of angles is necessary to accumulate backscattered rays simulated with the Monte Carlo method, while it is also important to collect as close to 0° in the backward direction as possible to obtain an accurate result [11]. The 2° range was chosen because, as reported in [11], $p(r)$ changes negligibly for angles of backscattering from 0° to 2°, while it differs for larger angles. A refractive index of 1.59 was used for the spheres and 1.33 for the medium. Single scattering events were excluded from the stored $p(r)$ distribution. The polarization-dependent phase function was calculated with Mie theory at $\lambda = 680$ and sampled with an angular resolution of $\pi/500$ radians. The Mie phase function is more accurate for modeling scattering from spherical particles than the often-used Henyey Greenstein phase function and allows for the simulation of polarization effects. The probability distribution for backscattered light was collected and (3) was applied to calculate the 2-D LEBS signal. The simulation modeled a thick slab geometry where less than 3% of the intensity was transmitted to the bottom of the slab. An infinitely narrow vertically polarized incident beam was propagated through the simulated random scattering medium with the Stokes vectors being tracked and stored once the beam reemerged to the top surface. For each simulation run, between 10^8 and 10^9 rays were stored to obtain the $p(r)$ for all of the four Stokes vectors. Mueller matrix multiplication was then used to obtain the copolarized distribution of $p(r)$. The grid resolution was maintained $<L_{SC}/20$ and the maximum collected r was maintained $>10L_{SC}$. This ensured that the error due to under sampling was small.

III. Results

A. LEBS Enhancement Factor

A comparison of the experimentally observed enhancement factor with the enhancement factor calculated from Monte Carlo simulation for a variety of spatial coherence lengths is shown in Fig. 3. A constant multiplicative coefficient of 0.5 was used to adjust the Monte Carlo enhancement factor for effects such as the contribution of the single scattering fraction and a finite spot size. Note that the selected polarization contribution to $p(r)$ is already taken into account in the Monte Carlo model by tracking the Stokes vectors and Mueller matrix multiplication of the collected signal. As seen in Fig. 3(a), the enhancement factor from experiment and simulation is higher for increasing L_{SC}. When the enhancement factor is plotted with $L_{SC}\mu_s^*$, as shown in Fig. 3(b), and the graphs collapse to a single monotonic relationship. This relationship can be approximated with a straight line for values of $L_{SC}\mu_s^* < 1$, which agrees with previous observed trends from LEBS Monte Carlo simulations [12]. In contrast, the enhancement factor measured with EBS has no

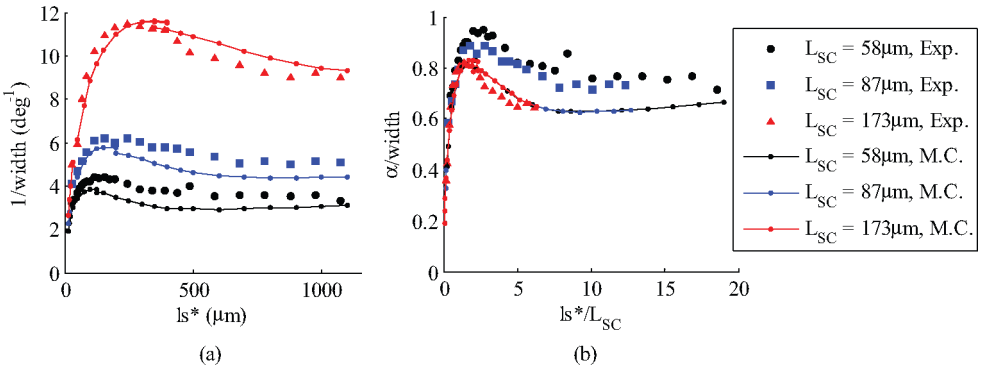

Fig. 4. LEBS width relationship with ls* and L_{SC}. (a) Inverse width dependence on spatial coherence length ($g = 0.86$) for Monte Carlo (lines) and experiment (symbols). (b) Data from (a) when the width is scaled by the angular extent of the source and ls* is scaled by the spatial coherence length.

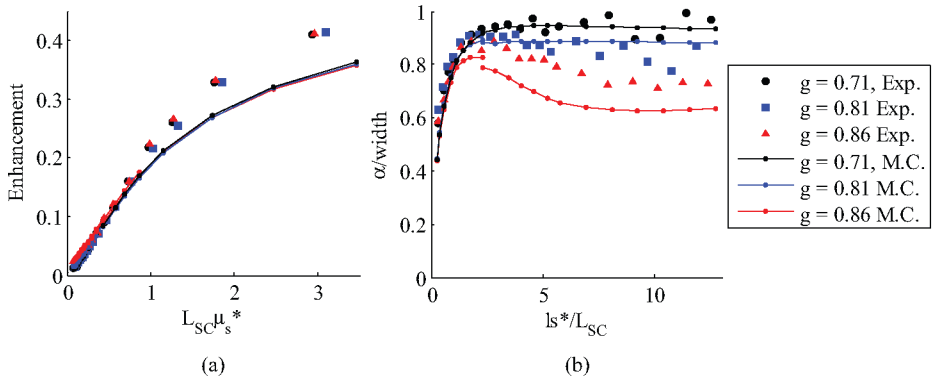

Fig. 5. Dependence of LEBS enhancement factor and width on ls* for phase functions with varying values of the anisotropy coefficient (g). The dependence of the enhancement factor (a) is approximately described through the value of $L_{\mathrm{SC}}\mu_s$. On the other hand, the LEBS width (b) has a more complicated relationship on the phase function when $\mathrm{ls}^* \gg L_{\mathrm{SC}}$. The relationships of both the enhancement factor and peak width are well-modeled with the Monte Carlo simulation.

relationship with the scattering coefficient. This result can be explained from considerations of the Fourier transform relationship of LEBS with $p(r)\cdot c(r)$. The LEBS enhancement factor is the integral of $p(r)\cdot c(r)$, $I_{\mathrm{LEBS}}(0) = \iint p(r)c(r)d^2r$. As ls* increases, $p(r)$ extends to larger distances and the area under $p(r)\cdot c(r)$ decreases. This is identical to reducing the extent of the degree of spatial coherence by decreasing L_{SC}. The dependence of the LEBS enhancement factor on the shape of the phase function ($g = 0.71$–0.86) is shown in Fig. 5(a). The dependence is seen to approximately characterize the μ_s^* of the sample.

B. LEBS Peak Width

The LEBS peak width, defined as the full-width at half maximum, is another important measurable parameter that has previously been shown to have fascinating characteristics for varying optical properties. Earlier experimental results suggest that the LEBS peak width may be used to measure subdiffusion optical properties such as the anisotropy factor g, the average cosine of the phase function. Indeed, by using a more accurate phase function to model the particle scattering, agreement between experiment and simulation is attained for the first time (see Fig. 4). Fig. 4(a) shows the inverse LEBS peak width as function of ls* for Monte Carlo simulation and experiment ($g = 0.86$) for three values of L_{SC}. The relationship between the peak width and L_{SC} is demonstrated in Fig. 4(b) by appropriately scaling the axes as α/width versus ls$^*/L_{\mathrm{SC}}$, where α is the angular extent of the source and can be calculated from (4). It is important to recognize that the shape of $p(r)$ is uniquely characterized by the α/width versus ls$^*/L_{\mathrm{SC}}$ dependence. In Fig. 5(b), the appropriately scaled width is shown for a variety of phase functions ($g = 0.71$–$g = 0.86$). Although, the LEBS peak width is related to λ/L_{SC} (i.e., α) at large ls$^*/L_{\mathrm{SC}}$ as predicted by [12], the LEBS width is also highly dependent on subdiffusion characteristics of the sample when $\mathrm{ls}*/L_{\mathrm{SC}} \gg 1$. These characteristics are determined by the shape of $p(r)$ at small values of r ($r/\mathrm{ls}^* < 1$).

Fig. 6(a) shows Monte Carlo simulation results compared with the diffusion approximation for LEBS, obtained from (2) and (5). The diffusion approximation for LEBS shows good agreement for $\mathrm{ls}^* < 2L_{\mathrm{SC}}$, but becomes far less accurate for $\mathrm{ls}*/L_{\mathrm{SC}} \gg 1$. This is because the diffusion approximation is a poor model of $p(r)$ for $r < \mathrm{ls}^*$. Fig. 6(a) also shows a comparison between the commonly used Henyey-Greenstein-phase-function-based Monte Carlo and the Mie-phase-function-based Monte Carlo for the same value of g. This demonstrates that the shape of the phase function plays an important role in the accuracy of the simulation. Finally, Fig. 6(b) shows the same Monte Carlo data observed in Fig. 6(a) when the LEBS peak is sampled with a spectrometer-based system that has been used to collect LEBS signals in prior work [4], [5], [7], [16]. This is simulated by averaging the peak in one angular dimension over a spectrometer slit width of 1.3α. Averaging over a slit width

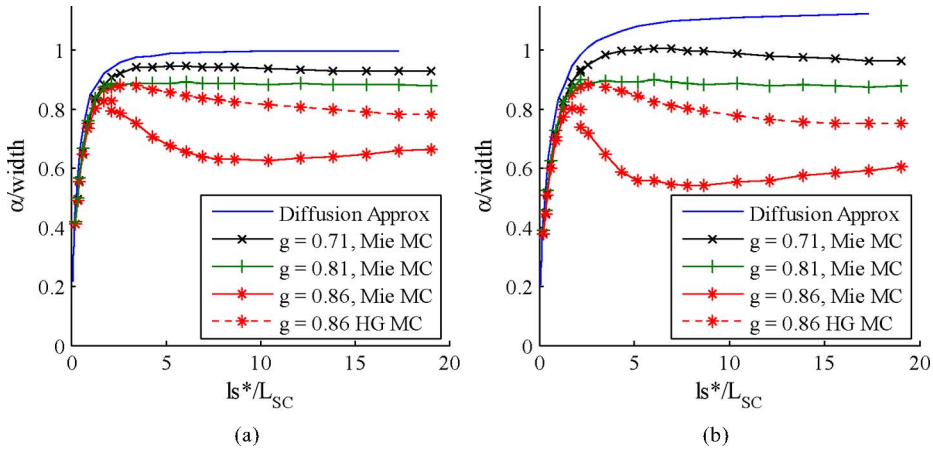

Fig. 6. Comparison of diffusion approximation of LEBS with Monte Carlo simulations utilizing various phase functions. (a) LEBS peak width agrees with the diffusion approximation for $\mathrm{ls}^* < L_{\mathrm{SC}}$. At $\mathrm{ls}^* \gg L_{\mathrm{SC}}$, the diffusion approximation is no longer accurate because it is not a good model for $p(r)$ for $r < \mathrm{ls}^*$. A comparison between the Mie and Henyey Greenstein phase function for the same value of g indicates that the accuracy of the phase function is important for modeling the LEBS peak width. (b) Same data are shown as in (a), but simulated for a spectrometer-based LEBS measurement where the spectrometer slit is of angular width 1.3α. In this case, the sensitivity due to varying phase functions at $\mathrm{ls}^* \gg L_{\mathrm{SC}}$ becomes more pronounced.

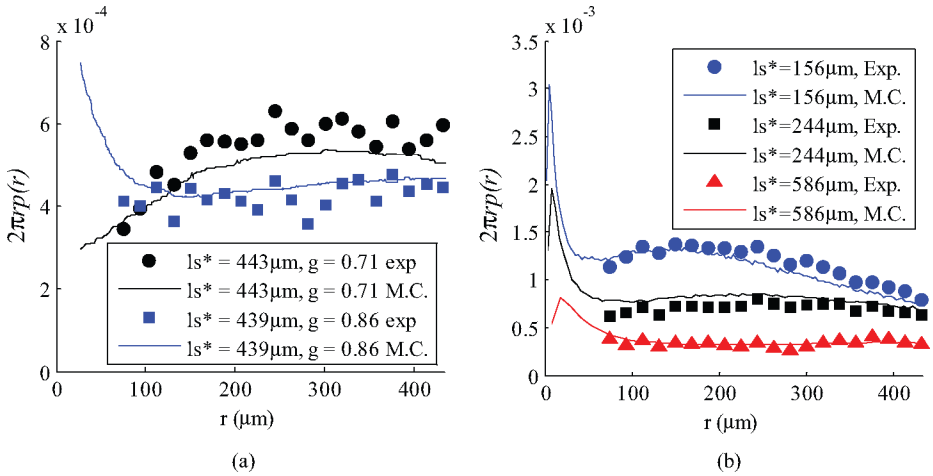

Fig. 7. Experimental measurements of $p(r)$ compared with Monte Carlo Simulation. (a) Comparison for two different values of g and similar values of ls^* is made between Monte Carlo and experimentally collected data. (b) Three values of ls^* are shown for $g = 0.86$. In all cases, experimentally calculated $p(r)$ curves agree well with Monte Carlo simulation.

amplifies the dependence of the peak width on the shape of the phase function for $\mathrm{ls}^* \gg L_{\mathrm{SC}}$.

C. Measurement of p(r) With LEBS

By applying (6), a measurement of $p(r)$ is possible by obtaining the inverse Fourier transform of the LEBS intensity distribution and dividing by the degree of spatial coherence. This was accomplished with the discrete 2-D inverse fast Fourier transform in MATLAB. The obtained $p(r)$ is a sharply decaying function that is better visualized after integration over the azimuth angle, resulting in the more commonly shown dependence of $2\pi rp(r)$. In principle, the calculation is valid from smallest value of r (determined by the collected angular range) up to the first zero of the spatial coherence function. Practically, the presence of noise limits the smallest and longest reliably measured r. The minimum reliable value of r is accurate from a resolution limit that is determined by the maximum angle of the $I_{\mathrm{LEBS}}(\theta)$ that is above the noise level. The maximum reliable value of r is the point where the noise level overcomes the degree of spatial coherence. Fig. 7 shows $2\pi rp(r)$ curves experimentally measured with LEBS compared with curves obtained from Monte Carlo simulations. The $2\pi rp(r)$ curves for two different particle sizes ($D = 0.36$ μm and $D = 0.65$ μm) have different behaviors for $r < \mathrm{ls}^*$ [see Fig. 7(a)]. For larger values of r, the governing parameter is ls^* and the curves are indistinguishable. Fig. 7(b) shows the changes in $p(r)$ when ls^* is varied. As anticipated, an increase in ls^* broadens $p(r)$ and reduces the probability at small radii.

Fig. 8 shows measurements of $2\pi rp(r)$ obtained from precancerous colonic rat tissue compared with healthy colonic rat tissue. The measurements were taken 10 weeks after either AOM or saline injection. In this animal model, colonic tumors normally develop 40 weeks after AOM injection. The colonic carcinogenesis process begins in the mucosa, a tissue layer that is <1 mm thick. Alterations in $p(r)$ at small radii suggest changes

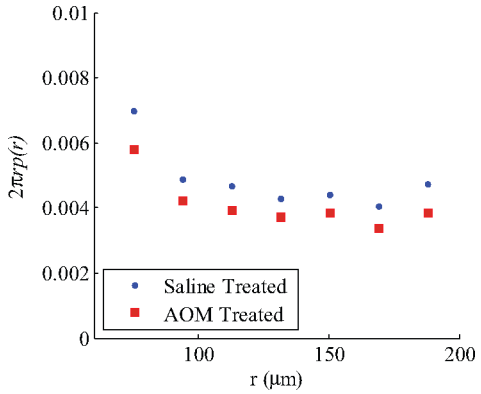

Fig. 8. Measurement of $p(r)$ from normal and AOM-treated precancerous rat tissue for ($L_{\mathrm{SC}} = 86\ \mu$m). Alterations in $p(r)$ at small length scales indicate that precancerous structural changes are present in the epithelial tissue of AOM-treated rats.

in the structure of the mucosal colonic tissue. Larger values of r correspond to more deeply penetrating light. In this case, the values of r are limited to small length scales such that the majority of the signal is confined to the epithelium. This isolation of epithelial signal is of great value for the detection of early precancer because most cancers originate due to the accumulation of mutations in epithelial tissue.

IV. Discussion and Conclusion

We have presented experimental data that validate the Monte Carlo model of LEBS for a broad range of optical properties. Polystyrene microspheres in water were used as samples, which were then simulated with Monte Carlo code that implements a phase function calculated with Mie theory and tracks the polarization state of each scattering event. The results obtained from the LEBS peak width, enhancement factor, and $p(r)$ show unprecedented agreement between experiment and simulation. These results suggest that LEBS measurements are highly sensitive to the shape of the phase function, contrasting the case of EBS, which is well modeled by the diffusion approximation. In particular, Fig. 5(b) illustrates the sensitivity of the LEBS width measurement to the anisotropy coefficient in the LEBS regime when $\mathrm{ls}^* \gg L_{\mathrm{SC}}$. As shown in Fig. 7, when the LEBS signal is converted to $p(r)$ for two different bead sizes (different phase functions), the difference in scattering at small values of r becomes apparent, while $p(r)$ at $r > \mathrm{ls}^*$ is insensitive to the shape of the phase function and simply determined by ls^*. The agreement between the experimentally measured $p(r)$ and that from Monte Carlo indicates that the measurement is accurate. In Fig. 8, the $p(r)$ measured using LEBS is shown from biological tissue measurements of control and carcinogen-treated rats. This tissue measurement of $p(r)$ is the first validated measurement of $p(r)$ using the enhanced backscattering technique.

A diffusion approximation for LEBS was presented and illustrated in Fig. 6. The LEBS diffusion approximation was reliable at $\mathrm{ls}^*/L_{\mathrm{SC}} < 1$, but quickly becomes inaccurate at longer values of ls^*. Fig. 6 also demonstrates the importance of the shape of the phase function. An identical value of g simulated with the Henyey Greenstein phase function results in different LEBS peak widths than those obtained from simulations with the Mie phase function. This underscores the importance of choosing an accurate phase function for LEBS simulation with Monte Carlo.

It is possible that the simulation results may be further improved by incorporating other considerations from the experimental setup. The Monte Carlo simulation models the propagation of light at a single wavelength, while in the experiment, the liquid-crystal-tunable filter (LCTF) has a 7 nm bandwidth. The interface between the air and water was not considered, and this may also improve the results [17]. Finally, it is possible that experimental errors such as the variation in shape or quality of the polystyrene microsphere suspensions limit the accuracy of the Mie phase function. In this case, the exact phase function must be measured experimentally in order to validate the Monte Carlo model of LEBS to a higher level of accuracy. One additional challenge in obtaining experimental LEBS measurements is an accurate fitting of the baseline. If angles that are too close to the peak are used to fit the baseline, oversubtraction may reduce the enhancement factor and narrow the peak width. On the other hand, noise considerations make baseline fitting at very large angles impractical. Finally, the assumption that the intensity throughout the secondary source is completely incoherent and perfectly uniform may be challenged. Any nonuniformity in the intensity distribution in the pinhole would result in an increased spatial coherence length. This effect would make the experimentally obtained peak widths have slightly narrower widths and higher enhancement factors and would be more problematic with larger apertures (shorter L_{SC}).

In summary, we have shown that experimental values of the LEBS enhancement factor and width are well modeled by the Monte Carlo method for a large range of optical properties. We have shown that the accuracy in the choice of the phase function has a large impact on the LEBS peak width when $\mathrm{ls}^* \gg L_{\mathrm{SC}}$. On the other hand, when $\mathrm{ls}^* < L_{\mathrm{SC}}$, the choice of the phase function is not important and the use of the diffusion approximation to model LEBS behavior is sufficient. Because LEBS peak is directly related to $p(r)$, this is consistent with a notion, which has been long held in the field of tissue optics: for $r > \mathrm{ls}^*$, light transport can be accurately modeled by the diffusion approximation (which depends on ls^* only and is independent of the phase function). On the other hand, the shape of the phase function has a profound effect for short, subdiffusion length scales of light propagation, i.e., $r \ll \mathrm{ls}^*$. These results also suggest that the LEBS peak width may be used to measure parameters of the phase function such as g. Moreover, we have demonstrated that the calculation of $p(r)$ at small length scales is feasible by performing an inverse Fourier transform of the LEBS signal. The $p(r)$ measurement from polystyrene microspheres showed good agreement between experiment and simulation. We then applied the $p(r)$ calculation to an animal model demonstrating that there may be potential differences in the $p(r)$ at small length scales between precancerous and healthy colonic rat tissue.

References

[1] M. P. Vanalbada and A. Lagendijk, "Observation of weak localization of light in a random medium," *Phys. Rev. Lett.*, vol. 55, pp. 2692–2695, 1985.

[2] E. Akkermans, P. E. Wolf, and R. Maynard, "Coherent backscattering of light by disordered media—Analysis of the peak line-shape," *Phys. Rev. Lett.*, vol. 56, pp. 1471–1474, Apr. 7, 1986.
[3] M. B. Vandermark, M. P. Vanalbada, and A. Lagendijk, "Light-scattering in strongly scattering media—Multiple-scattering and weak localization," *Phys. Rev. B*, vol. 37, pp. 3575–3592, Mar. 1, 1988.
[4] Y. L. Kim, Y. Liu, V. M. Turzhitsky, H. K. Roy, R. K. Wali, and V. Backman, "Coherent backscattering spectroscopy," *Opt. Lett.*, vol. 29, pp. 1906–1908, Aug. 15, 2004.
[5] Y. L. Kim, Y. Liu, V. M. Turzhitsky, R. K. Wali, H. K. Roy, and V. Backman, "Depth-resolved low-coherence enhanced backscattering," *Opt. Lett.*, vol. 30, pp. 741–743, Apr. 1, 2005.
[6] H. Subramanian, P. Pradhan, Y. L. Kim, and V. Backman, "Penetration depth of low-coherence enhanced backscattered light in subdiffusion regime," *Phys. Rev. E*, vol. 75, pp. 041914-1–041914-9, Apr. 2007.
[7] Y. L. Kim, Y. Liu, R. K. Wali, H. K. Roy, and V. Backman, "Low-coherent backscattering spectroscopy for tissue characterization," *Appl. Opt.*, vol. 44, pp. 366–377, Jan. 20, 2005.
[8] H. K. Roy, V. Turzhitsky, Y. Kim, M. J. Goldberg, P. Watson, J. D. Rogers, A. J. Gomes, A. Kromine, R. E. Brand, M. Jameel, A. Bogovejic, P. Pradhan, and V. Backman, "Association between rectal optical signatures and colonic neoplasia: Potential applications for screening," *Cancer Res.*, vol. 69, pp. 4476–4483, May 15, 2009.
[9] Y. Liu, R. E. Brand, V. Turzhitsky, Y. L. Kim, H. K. Roy, N. Hasabou, C. Sturgis, D. Shah, C. Hall, and V. Backman, "Optical markers in duodenal mucosa predict the presence of pancreatic cancer," *Clin. Cancer Res.*, vol. 13, pp. 4392–4399, Aug. 1, 2007.
[10] V. Turzhitsky, Y. Liu, N. Hasabou, M. Goldberg, H. K. Roy, V. Backman, and R. Brand, "Investigating population risk factors of pancreatic cancer by evaluation of optical markers in the duodenal mucosa," *Disease Markers*, vol. 25, pp. 313–321, 2008.
[11] H. Subramanian, P. Pradhan, Y. L. Kim, Y. Liu, X. Li, and V. Backman, "Modeling low-coherence enhanced backscattering using Monte Carlo simulation," *Appl. Opt.*, vol. 45, pp. 6292–6300, Aug. 20, 2006.
[12] M. Xu, "Low-coherence enhanced backscattering beyond diffusion," *Opt. Lett.*, vol. 33, pp. 1246–1248, Jun. 1, 2008.
[13] M. Born, E. Wolf, and A. B. Bhatia, *Principles of Optics : Electromagnetic Theory of Propagation, Interference and Diffraction of Light*, 7th (expanded) ed. Cambridge, U.K./New York: Cambridge Univ. Press, 1999.
[14] J. C. Ramella-Roman, S. A. Prahl, and S. L. Jacques, "Three Monte Carlo programs of polarized light transport into scattering media: Part I," *Opt. Exp.*, vol. 13, pp. 4420–4438, Jun. 13, 2005.
[15] J. C. Ramella-Roman, S. A. Prahl, and S. L. Jacques, "Three Monte Carlo programs of polarized light transport into scattering media: Part II," *Opt. Exp.*, vol. 13, pp. 10392–10405, Dec. 12, 2005.
[16] Y. L. Kim, V. M. Turzhitsky, Y. Liu, H. K. Roy, R. K. Wali, H. Subramanian, P. Pradhan, and V. Backman, "Low-coherence enhanced backscattering: Review of principles and applications for colon cancer screening," *J. Biomed. Opt.*, vol. 11, p. 041125, Jul./Aug. 2006.
[17] M. Ospeck and S. Fraden, "Influence of reflecting boundaries and finite interfacial thickness on the coherent backscattering cone," *Phys. Rev. E*, vol. 49, pp. 4578–4589, May 1994.

Vladimir Turzhitsky received the B.S. in biomedical engineering from Rensselaer Polytechnic Institute, Troy, NY, in 2004, and the M.S. and Ph.D. degrees in biomedical engineering from Northwestern University, Evanston, IL, in 2006 and 2009, respectively.

He is currently a Postdoctoral Fellow in the Department of Biomedical Engineering, Northwestern University. He has been involved in the development and characterization of low-coherence enhanced backscattering spectroscopy (LEBS), polarization-gating spectroscopy for the early detection of colon and pancreatic cancer. His current research interests include the understanding of light scattering phenomena under partial coherence illumination conditions and the application of these phenomena as cancer detection and screening techniques.

Jeremy D. Rogers received the B.S. degree in physics from Michigan Technological University, Houghton, MI, in 1999, and the M.S. and Ph.D. degrees in optical sciences from the College of Optical Sciences, University of Arizona, Tucson, in 2003 and 2006, respectively.

He was with NanoSciences Corporation, Oxford, CT, and was an Intern at Sandia National Laboratories, Albuquerque, NM. He is currently a Postdoctoral Fellow in biomedical engineering at Northwestern University, Evanston. His current research interests include theoretical and numerical modeling of light scattering as well as lens design and instrumentation for basic investigation and application of optical detection techniques.

Nikhil N. Mutyal received the B.Sc. and M.Sc. degrees in chemistry from the Indian Institute of Technology Kanpur, Kanpur, India. He is currently working toward the Ph.D. degree in biomedical engineering at Northwestern University, Evanston, IL.

His current research interests include finding new markers and therapeutics for the diagnosis and treatment of cancer, and finding the biological origins of changes in optical properties in the progression of cancer and developing instrumentation (fiber-optic probes) to detect these changes using low-coherence enhanced backscattering spectroscopy.

Hemant K. Roy received the B.S. degree (*summa cum laude*) in molecular biology from Vanderbilt University, Nashville, TN, in 1985, and the M.D. degree with distinction from Northwestern University, Evanston, IL, in 1989.

He completed his internal medicine training at Beth Israel Hospital/Harvard Medical School, Cambridge, MA, in 1992, and gastroenterology training at the University of Chicago, Chicago, IL, from 1992 to 1995. His current research interests include colon cancer prevention. He is engaged in the investigation of noncyclooxygenase mechanisms for apoptosis from nonsteroidal antiinflammatory agents and has been one of the pioneers the use of polyethylene glycol in chemoprevention. His translational group works on development of novel colorectal cancer screening strategies. He is currently a Clinical Associate Professor of medicine at the University of Chicago, Pritzker School of Medicine, Chicago, IL. He is also at NorthShore University HealthSystems, Evanston, IL, where he is the Director of Research and the Vice Chair of the section of Gastroenterology and the Duckworth Chair of Cancer Research.

Vadim Backman received the Ph.D. degree in medical engineering from Harvard University, Cambridge, MA, and Massachusetts Institute of Technology, Cambridge, in 2001.

He is currently a Professor of biomedical engineering at Northwestern University, Evanston, IL, a Program Leader in cancer bioengineering, nanotechnology and chemistry at the Robert H. Lurie Comprehensive Cancer Institute, Chicago, IL, and a member of the Professional Staff in the Division of Gastroenterology, NorthShore University HealthSystems, Evanston. He is engaged in translational research, which is focused on bridging these technological and biological innovations into clinical practice. His current research interests include biomedical optics, spectroscopy, microscopy, development of analytical approaches to describe light transport in biological media, and optical microscopy for nanoscale cell analysis.

Dr. Backman is the recipient of numerous awards, including being selected as one of the top 100 young innovators in the world by the Technology Review Magazine and the National Science Foundation CAREER Award.